# SPECT Imaging of Fluorine-18

Peter K. Leichner, Hugh T. Morgan, Karen P. Holdeman, Katherine A. Harrison, Frank Valentino, Roger Lexa, Richard F. Kelly, William G. Hawkins and Glenn V. Dalrymple

*Department of Radiology, University of Nebraska Medical Center, Omaha, Nebraska; and Picker International, Inc., Bedford Heights, Ohio*

The objective of this work was to determine the potential clinical usefulness of SPECT to image 511-keV annihilation photons. **Methods:** A triple-headed gamma camera equipped with ultrahigh-energy collimators was used to image $^{18}F$. Sensitivity measurements were carried out and the FWHM and FWTM were determined in air and for a unit-density scattering medium. Additionally, tomographic phantom studies were acquired to evaluate image quality. **Results:** The sensitivities of the three cameras were, for all practical purposes, identical. At a source-to-collimator distance of 100 mm, the FWHM and FWTM were 13 and 29 mm, respectively. A tomographic phantom study demonstrated that spheres with a diameter of 20 mm were well resolved when filled with $^{18}F$ activity and placed inside a water-filled phantom. **Conclusion:** The triple-headed SPECT camera in this investigation is a practical means of acquiring tomographic $^{18}F$ images. The reconstructed slices were of sufficient quality to be of value in some clinical studies.

**Key Words:** single-photon emission computed tomography; fluorine-18-FDG; collimation

**J Nucl Med 1995; 36:1472–1475**

In recent years, considerable progress has been made in developing better imaging devices and improved reconstruction software for SPECT. In particular, the introduction of dual- and triple-headed systems with stable gantries has enhanced the role of SPECT in clinical nuclear medicine and nuclear medicine research (*1*). As part of an ongoing research effort in radioimmunotherapy (RIT), we previously reported (*2*) SPECT imaging of $^{87}Y$ 485-keV photons with the Picker Prism 3000 (Picker International, Inc., Bedford Heights, OH). In that study, the feasibility of quantitative SPECT for $^{87}Y$ was demonstrated and this opened up the possibility of imaging $^{87}Y$-labeled antibodies for treatment planning of RIT with $^{90}Y$-labeled antibodies.

The purpose of the present work was to determine the potential usefulness of the Prism 3000 for metabolic imaging of pharmaceuticals labeled with positron emitters. Metabolic imaging of positron-emitting radiopharmaceuticals has proven its clinical value in several disciplines, including cardiology (*3,4*), psychiatry (*5,6*) and oncology (*7–11*). The sensitivity and spatial resolution of SPECT systems for 511-keV photons are lower than those of PET scanners. Additionally, attenuation correction in PET imaging is more rigorous than for SPECT. There are, however, practical advantages associated with SPECT devices capable of imaging high-energy photons. These include considerable reductions in equipment cost and space requirements because one imaging device may potentially be useful for imaging photons of all energies that are of interest in clinical nuclear medicine. Additionally, SPECT cameras are more commonly used than PET scanners so that SPECT imaging will result in increased access to diagnostic studies that utilize positron-emitting radiopharmaceuticals.

## MATERIALS AND METHODS

### SPECT System and Collimation

The Picker Prism 3000 is a triple-headed SPECT system for brain and body tomography. Each head is equipped with a rectangular NaI(Tl) crystal (292 × 438 × 9.5 mm) that encompasses a useful field-of-view of dimensions 240 × 400 mm. Ultrahigh-energy parallel-hole collimators for 511-keV photons were designed with a tunnel length of 77.0 mm with hexagonal holes arranged in a hexagonal-packed pattern. This design helps maintain the system's sensitivity in spite of the relatively long bore. The diameter of the hexagonal holes is 5.08 mm (flat side to flat side) with a septal thickness of 3.43 mm. The collimator cores are mounted in an all-lead frame designed for 511-keV photons. The mass of each collimator assembly is 100 kg so that the system's gantry supports 300 kg of collimator mass during imaging procedures with 511-keV photons.

### Sensitivity and Resolution Measurements

A 15% energy window, centered at 511 keV, was used in all planar and tomographic image acquisitions and measurements. All filtering of planar projection data or reconstructed slices and all reconstructions were carried out using the system's software.

The sensitivity of each of the three heads equipped with the ultrahigh-energy collimators was determined by placing a flat source (tissue culture flask) containing 21.7 MBq (0.587 mCi) $^{18}F$ in water sequentially on each collimator. A total of 100 kcts was acquired for each head. For purposes of comparison, a second flask containing 6.66 MBq (0.180 mCi) $^{99m}Tc$ was subsequently used to also measure the sensitivity for this radionuclide.

Measurements of the FWHM and FWTM of the point-spread function for camera 1 were made in air and with a unit density

Received May 11, 1994; revision accepted Nov. 10, 1994.
For correspondence or reprints contact: Peter K. Leichner, PhD, Department of Radiology, University of Nebraska Medical Center, Omaha, NE 68198-1045.

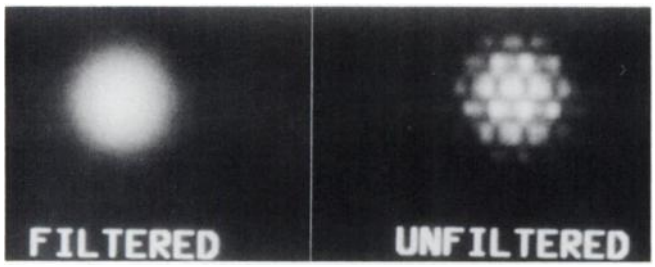


**FIGURE 1.** Filtered and unfiltered images of the point source in air at a source-to-collimator distance of 200 mm.

scattering medium. A point source of $^{18}F$ was prepared by filling a hollow plastic sphere, 1 cm in diameter, with $^{18}F$ activity and water. Images of this source were acquired at source-to-collimator distances of 20, 30 and 40 cm. At these relatively large distances, the effect of the finite size of the point source was small and measurements were extrapolated to smaller distances using a linear regression analysis. The effect of a scattering medium on the point spread function was determined at a fixed source-to-collimator distance of 20 cm. Rectangular plastic sheets, 56 cm × 44 cm and 1.27 cm in thickness, were placed between the source and collimator with the source centered under the sheets. Images were acquired for thicknesses of 3.8, 7.6, 11.4 and 15.2 cm. All images were acquired in 128 × 128 matrices and a fixed acquisition time of 300 sec. The total number of counts in the images ranged from about 1.5 million to over 230,000 counts.

The raw images of the $^{18}F$ point sources required filtering because the septal thickness (3.43 mm) was approximately the same size as the intrinsic resolution of the camera system (3–4 mm). This produced a high-frequency, two-dimensional spatially periodic pattern (Fig. 1). The spatial frequency of the grid pattern was approximately the reciprocal of the hole size or 1.97 $cm^{-1}$. The FWHM at 200 mm, the smallest source-to-collimator distance used for measurements, was 2.3 cm, representing a spatial frequency of 0.434 $cm^{-1}$. On the collimator surface, it was 0.59 cm, corresponding to a spatial frequency of 1.69 $cm^{-1}$. Therefore, the use of a smoothing filter with a high cutoff frequency for all practical purposes introduced no error. This was verified by the fact that after a certain point (order = 16, cutoff > 0.31 $pixels^{-1}$) varying the order parameter of the Butterworth filter caused no change in FWHM or FWTM but almost entirely eliminated the grid pattern. Hence, the order paramater was set as high as possible to eliminate only the grid pattern from the images. Filtered and unfiltered images of the point source in air at a source-to-collimator distance of 200 mm are shown in Figure 1. The filtered images were analyzed to obtain numerical values of the FWHM and FWTM.

### Tomographic Phantom Studies

A cylindrical SPECT phantom (Data Spectrum Corp., Chapel Hill, NC) with an inside diameter of 21.6 cm and an inside height of 18.6 cm was utilized in tomographic phantom studies. In one phantom study, six hollow spheres with diameters of 1, 1.3, 1.6, 2.1, 2.8 and 3.4 cm, respectively, were filled with $^{18}F$ activity and mounted inside the phantom. The phantom was filled with plain water to provide a scattering medium. Planar projection data were acquired in 3° angular intervals (40 steps for each camera) with an acquisition time of 30 sec/frame. Raw data were acquired in 128 × 128 matrices. The raw data were corrected for uniformity and prefiltered using the system's Wiener filter with a default multiplier of 1. In reconstructions, the grid pattern produced no artifacts because the spatial frequency of the grid pattern was beyond the cutoff frequency of the filters employed. Transverse slices were generated from the prefiltered data and attenuation-corrected using a linear attenuation coefficient of 0.079 $cm^{-1}$. In all tomographic reconstructions, a slice thickness of 1 pixel was chosen (7.12 mm for 64 × 64 matrices and 3.56 mm for 128 × 128 matrices).

In a second phantom study, two plastic containers with a diameter of 7.3 cm and a volume of 530 ml were taped to the inside of the SPECT phantom. One of the containers was filled with $^{18}F$ activity and water at a concentration of 287 kBq/ml (7.77 μCi/ml) and the second container was filled with plain water. The SPECT phantom was filled with $^{18}F$ activity and water at a concentration of 57 kBq/ml (1.54 μCi/ml). This phantom therefore simulated hot and cold lesions in a scattering medium that contained a background of activity. In view of the larger volumes of this phantom, planar projection data were acquired in 64 × 64 matrices. Acquisition and reconstruction protocols for these data were the same as those previously described.

For comparison, a SPECT acquisition of the same phantom was carried out using a conventional high-energy, parallel-hole collimator (rated at 400 keV). The parameters of the high-energy collimator were hole size 3.81 mm, septal thickness 1.73 mm and hole length 58.4 mm. Acquisition and reconstruction protocols were the same as those used with the ultrahigh-energy collimator.

## RESULTS AND DISCUSSION

The results of sensitivity measurements in units of counts per second per 37 kBq (cps/μCi) for $^{18}F$ and $^{99m}Tc$

**TABLE 1**
Sensitivity (cps/37 kBq or cps/μCi) of the SPECT System Equipped with Ultrahigh Energy Collimators

| Radionuclide | Camera 1 | Camera 2 | Camera 3 |
|---|---|---|---|
| $^{18}F$ | 2.04 | 1.98 | 1.98 |
| $^{99m}Tc$ | 2.31 | 2.29 | 2.28 |

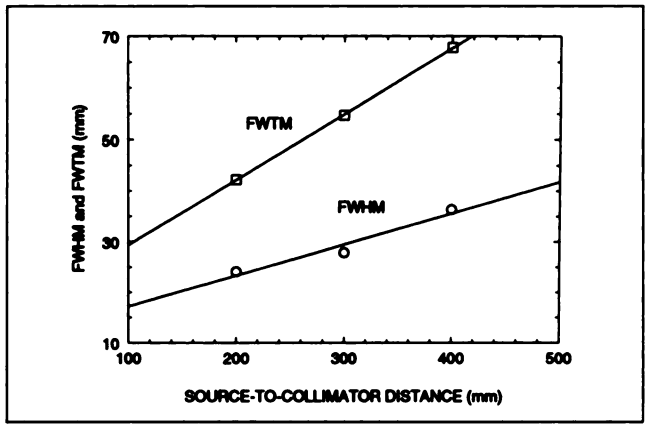


**FIGURE 2.** FWHM and FWTM in air as a function of source-to-collimator distance. The lines connecting the data points represent the results of a linear regression analysis used to determine the FWHM and FWTM at a source-to-collimator distance of 100 mm and on the collimator surface.

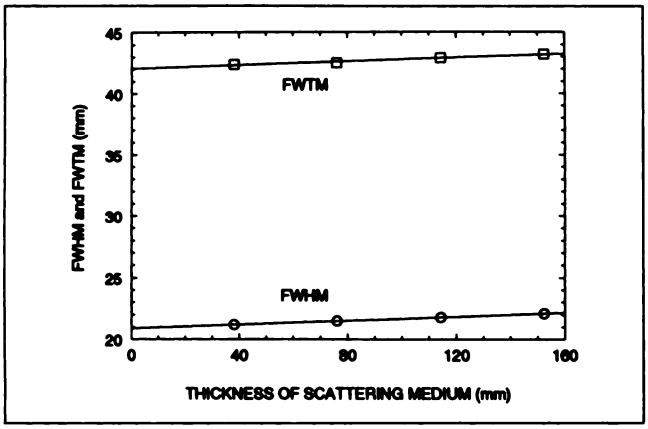


**FIGURE 3.** FWHM and FWTM at a constant source-to-collimator distance for four thicknesses of unit-density scattering medium. The lines connecting the data points represent the results of a linear regression analysis.

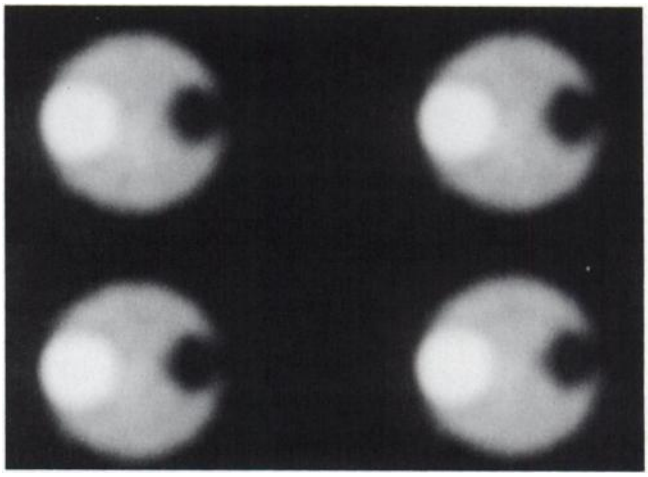

**FIGURE 5.** Representative set of transverse slices of the SPECT phantom that simulates a hot and cold lesion in a background of activity. The raw data were acquired with the ultrahigh-energy collimators.

are summarized in Table 1. For all practical purposes, the sensitivity of the three cameras was the same and the sensitivity for $^{18}F$ was 87% of that for $^{99m}Tc$.

Measurements of the FWHM and FWTM in air and for the scattering medium are summarized in Figures 2 and 3, respectively. When the measurements in air were extrapolated to a source-to-collimator distance of 100 mm, the FWHM and FWTM were 17 and 29 mm, respectively. Extrapolation to the collimator surface yielded FWHM = 5.9 mm and FWTM = 16 mm. These results were consistent with measurements of the resolution parameters of other collimators rated for 511-keV photons (*12*). The data in Figures 2 and 3 also show that increases in FWHM and FWTM depend strongly on source-to-collimator distance but only weakly on the thickness of the scattering medium. Increases in the resolution parameters for 511-keV photons were therefore principally due to geometric effects.

A transverse slice of the SPECT phantom containing six hollow spheres filled with $^{18}F$ activity is shown in Figure 4. All six spheres were visualized. A set of representative transverse slices of the second phantom study generated from raw data acquired with the ultrahigh-energy collimator is shown in Figure 5. The hot and cold lesions (7.3 cm in diameter) and the activity background were easily distinguished and well defined. The image of the hot lesion is larger than that of the cold lesion. The size of the hot lesion is overestimated and the size of the cold lesion is underestimated because of the finite resolution of the detection system. An identical set of transverse slices of this phan-

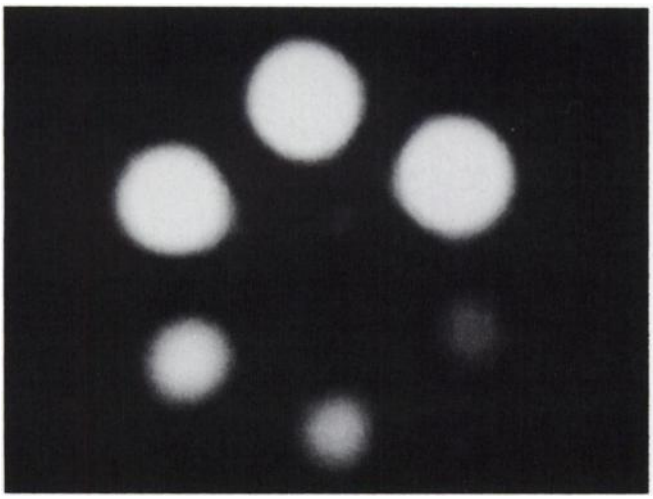

**FIGURE 4.** A transverse slice of the SPECT phantom containing six spheres of diameters 1, 1.3, 1.6, 2.1, 2.8 and 3.4 cm immersed in plain water as a scattering medium.

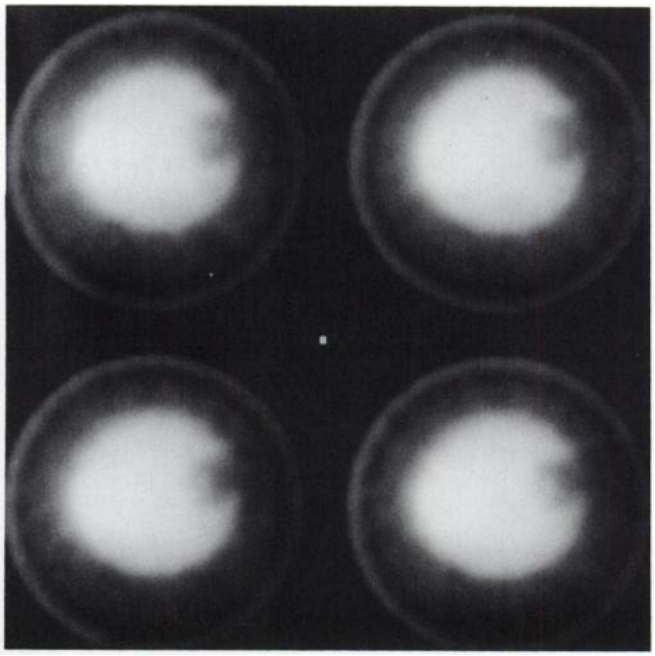

**FIGURE 6.** The same set of transverse slices as in Figure 4, but in this case the raw data were acquired with conventional high-energy collimators. The imaged phantom extends over the total field of view of the cameras because of the extent of septal penetration.

tom, but generated from image data acquired with the conventional high-energy collimator, is presented in Figure 6. The data in Figure 5 illustrate that septal penetration of the ultrahigh-energy collimator by 511-keV photons was minimal, resulting in good image quality. In contrast, Figure 6 demonstrates considerable septal penetration of the conventional high-energy collimator and consequent image degradation.

Overall, the results of this study show that SPECT imaging of 511-keV photons with a triple-headed gamma camera is feasible and that septal penetration of the ultrahigh-energy collimator is minimal.

## ACKNOWLEDGMENT

This work was supported in part under U.S. Department of Energy grant DE-FG02-91ER61195.

## REFERENCES

1. Juni JE. Doing well under pressure: dedicated SPECT cameras come of age. *J Nucl Med* 1993;34:1789–1792.
2. Leichner PK, Harvey EB, Holdeman KP, et al. SPECT imaging of $^{87}Y$ (485-keV) photons [Abstract]. *Antibody Immunoconj Radiopharm* 1992;5: 355.
3. Schwaiger M, Hicks R. The clinical role of metabolic imaging of the heart by positron emission tomography. *J Nucl Med* 1991;32:565–578.
4. Gould KL. PET perfusion imaging and nuclear cardiology. *J Nucl Med* 1991;32:579–606.
5. Fukuyama H, Ogawa M, Yamauchi H, et al. Altered cerebral energy metabolism in Alzheimer's disease: a PET study. *J Nucl Med* 1994;35:1–6.
6. Kippenhan JS, Barker WW, Nagel J, Grady C, Duara R. Neural-network classification of normal and Alzheimer's disease subjects using high-resolution and low-resolution PET cameras. *J Nucl Med* 1994;37:7–15.
7. Coleman RE, Hoffman JM, Hanson MW, Sostman HD, Schold SC. Clinical application of PET for the evaluation of brain tumors. *J Nucl Med* 1991;32: 616–622.
8. Strauss LG, Conti PS. The applications of PET in clinical oncology. *J Nucl Med* 1991;32:623–648.
9. Paul R. Comparison of fluorine-18-2-fluorodeoxyglucose and gallium-67 citrate imaging for detection of lymphoma. *J Nucl Med* 1987;28:288–292.
10. Kuwabara Y, Ichya Y, Otsuka M, et al. High [$^{18}F$]FDG uptake in primary cerebral lymphoma: a PET study. *J Comput Assist Tomogr* 1988;12:47–48.
11. Okada J, Joshikawa K, Imazeki K, et al. Comparison of fluorine-18-FDG and gallium-67 in malignant lymphoma. *J Nucl Med* 1990;31:888.
12. Clarke LP, Cullom SJ, Shaw R, et al. Bremsstrahlung imaging using the gamma camera: factors affecting attenuation. *J Nucl Med* 1992;33:161–166.